Temperature-pressure phase diagram and electronic properties of the organic metal κ-$(BETS)_2Mn[N(CN)_2]_3$

V. N. Zverev,[1,2] M. V. Kartsovnik,[1] W. Biberacher,[1] S. S. Khasanov,[2] R. P. Shibaeva,[2] L. Ouahab,[3] L. Toupet,[4] N. D. Kushch,[5] E. B. Yagubskii,[5] and E. Canadell[6]

[1]*Walther-Meissner-Institut, Bayerische Akademie der Wissenschaften, Garching, Germany*

[2]*Institute of Solid State Physics, Russian Academy of Sciences, Chernogolovka, Moscow region 142432, Russia*

[3]*Organométalliques et Matériaux Moléculaires, UMR 6226 CNRS-UR1, Sciences Chimiques de Rennes, Université de Rennes 1, 35042 Rennes Cedex, France*

[4]*Institut de Physique de Rennes, UMR 6251 CNRS-UR, Université de Rennes 1, 35042 Rennes Cedex, France*

[5]*Institute of Problems of Chemical Physics, Russian Academy of Sciences, Chernogolovka, Moscow region 142432, Russia*

[6]*Institut de Ciència de Materials de Barcelona, CSIC, Campus de la U.A.B., E-08193 Bellaterra, Spain*

(Received 28 May 2010; published 18 October 2010)

The crystal and electronic band structures as well as the transport properties of the recently synthesized layered radical cation salt κ-$(BETS)_2Mn[N(CN)_2]_3$ are investigated. It is shown that this salt is more anisotropic in the plane of conducting layers than other κ phases, a feature which noticeably influences its physical behavior. A phase transition resulting in the formation of an incommensurate superstructure below 102 K has been found. At temperature below 30 K a metal-insulator transition is observed. We argue that the transition is associated with electronic interactions rather than with structural changes. The T-P phase diagram has been studied under ^{4}He gas pressure up to 2.5 kbar. At moderately high pressure $P \approx 0.5$ kbar the metal-insulating transition is suppressed and the crystal becomes superconducting with $T_c \approx 5.7$ K. In the pressurized metallic state, Shubnikov-de Haas oscillations have been found, revealing a very small closed Fermi surface with a high-effective cyclotron mass influenced by many-body interactions.

DOI: 10.1103/PhysRevB.82.155123 PACS number(s): 74.70.Kn, 71.30.+h, 71.18.+y, 61.50.Ks

I. INTRODUCTION

Most of conducting systems of current interest, such as high-T_c cuprate and iron-pnictide superconductors,[1,2] organic conductors,[3] heavy fermion compounds,[4] and many others are characterized by low dimensionality, strong electronic correlations and, consequently, various competing ordering instabilities. In this respect, organic charge transfer salts of bis(ethylenedithio)tetrathiafulvalene (BEDT-TTF) and its derivatives, demonstrating generally a very high-crystal quality and possessing rather simple Fermi surfaces, are excellent model objects for studying correlation induced instabilities of the normal metallic state. In particular, κ-$(BEDT\text{-}TTF)_2X$ salts with polymeric anions have been of great interest, representing textbook examples of tunable Mott-insulating[5–7] and quantum spin-liquid[8,9] systems. Another trend developing rapidly in the last years is the synthesis and investigation of hybrid multifunctional molecular compounds combining conducting and magnetic properties. Since the spins of the conducting network are polarized by magnetic layers in these materials, they are regarded as promising candidates for molecular spin electronics (spintronics). The research in this direction has recently increasingly focused on the family of low-dimensional conductors based on radical cation salts of organic π donors with paramagnetic metal complex anions.[10] In such materials, conductivity is associated with electrons in organic layers whereas magnetism usually originates from localized spins of transition metal ions in insulating counterion layers. In particular, salts of BEDT-TTF and its selenium-substituted derivative bis(ethylenedithio)tetraselenafulvalene (BETS) have been shown to combine superconducting and paramagnetic[11] and even antiferromagnetic[12,13] properties. Moreover, interaction between localized spins in insulating magnetic layers and itinerant spins in conducting organic layers was found to lead to new fascinating phenomena such as field-induced superconductivity observed on κ-$(BETS)_2FeCl_4$ (Ref. 14) and κ-$(BETS)_2FeBr_4$.[15]

The recently synthesized layered conductor κ-$(BETS)_2Mn[N(CN)_2]_3$ (Ref. 16) is expected to combine interesting magnetic properties due to the presence of Mn^{2+} ions with strong electron correlations characteristic of a narrow half-filled conducting band of organic layers. This material undergoes at low temperatures a metal-insulator transition which is also reflected in its magnetic properties. It is, thus, a good candidate for studying synergism of the two classes of phenomena. It was also found that the insulating state can easily be suppressed, giving way to a superconducting state, if the sample is cooled inside a drop of silicone oil. This suggests high sensitivity of electronic properties to pressure. Aiming to determine the phase diagram of this compound and elucidate the nature of its electronic ground states, we have performed detailed studies of its crystal and electronic structures at low temperatures as well as its resistive behavior at different pressures and magnetic fields. We have found that the electronic structure of this phase exhibits some notable differences with respect to those of usual κ phases which are associated with a higher in-plane anisotropy of the partially filled bands. This feature, together with the occurrence of an incommensurate modulation at 102 K, profoundly affects the physical behavior of this salt, as made clear through the present transport and magnetotransport studies.

TABLE I. Crystal-structure data for κ-$(BETS)_2Mn[N(CN)_2]_3$, $C_{26}H_{16}N_9S_8Se_8Mn$, $M=1397.58$.

T (K)	200	110	88[a]	15[a]
Cell setting	Monoclinic	Monoclinic	Monoclinic	Monoclinic
Space group, Z	$P2_1/c$, 2	$P2_1/c$, 2	$P2_1/c$, 2	$P2_1/c$, 2
a (Å)	19.4723(9)	19.4130(11)	19.4281(8)	19.421(3)
b (Å)	8.4135(4)	8.3859(4)	8.3793(3)	8.3460(10)
c (Å)	11.9608(7)	11.8827(5)	11.8689(5)	11.8300(10)
α (deg)	90	90	90	90
β (deg)	92.315(4)	92.573(4)	92.665(4)	92.900(10)
γ (deg)	90	90	90	90
Cell volume (Å^3)	1957.94(17)	1932.50(16)	1930.09(13)	1915.0(4)
ρ (Mg/m^3)	2.371	2.402	2.405	2.424
μ, mm^{-1}	8.237	8.346	8.356	8.422
Refls collected/unique	22765/4627	32572/6280	21951/6263	34033/6197
Refls, $I>2\sigma$(I)	3781	5279	5300	4500
R_{int}	0.613	0.478	0.345	0.0693
θ_{max} (deg)	27.88	31.25	31.24	32.03
Parameters refined	278	259	259	259
Final R_1, $wR_2[I>2\sigma(I)]$	0.0319, 0.0850	0.0240, 0.0561	0.0226, 0.0540	0.0430, 0.1106
Goodness-of-fit	1.000	1.036	1.017	0.965

[a]Data are given for the averaged structure.

II. EXPERIMENTAL

A. Sample synthesis

Crystals of κ-$(BETS)_2Mn[N(CN)_2]_3$ were obtained by electrooxidation of BETS (10^{-3} M/l) in 1.1.2-trichloroethane +10%(vol) ethanol (96%) at constant current at 25 °C. The electrocrystallization conditions were the following: $I=0.5$ μA, $\tau=20-30$ days, electrolyte $Mn[N(CN)_2]_2(5.9\times10^{-3}$ M/l). The major product was $(BETS)_2[N(CN)_2]\cdot 2\ H_2O$ which appeared in the form of needlelike crystals one day after the beginning of the synthesis. Hexagonlike crystals of κ-$(BETS)_2Mn[N(CN)_2]_3$ started to grow after 1–2 weeks and were a minor fraction of the total yield.

B. X-ray crystallography

X-ray experimental data were collected on a single crystal ($0.25\times0.18\times0.08$ mm^3) at 200, 110, and 88 K using an Oxford Diffraction Gemini-R diffractometer equipped with a Ruby CCD detector and at 15 K using Oxford Diffraction Xcalibur diffractometer with CCD Sapphire 3 detector [λ(Mo K_α)=0.71073 Å, graphite monochromator and ω scans for both series]. Unit-cell parameters were refined with x-ray diffraction data collected using Cu K_α radiation (λ =1.54178 Å) for 200, 110, 88 K and Mo K_α radiation for 15 K. Data reduction with empirical absorption correction of experimental intensities (SCALE3ABSPACK program) was made with the CRYSALISPRO software.[17] The structure was solved by a direct method followed by Fourier synthesis and refined by a full-matrix least-squares method in an anisotropic approximation for all nonhydrogen atoms, with the SHELX-97 programs.[18] The staggered and eclipsed conformations of the terminal ethylene group occupancies were refined as constrained parameters to keep total occupancy equal unity. The staggered conformer occupancy parameter was refined to increase gradually when cooling and to be close unity at 88 K, consequently the eclipsed conformer occupancy to be negligible low. The positions of the H atoms were calculated geometrically in the terminal ethylene parts of BETS. Unit-cell parameters and details of data collection and refinement are summarized in Table I. CCDC 775974–775977 contain all the crystallographic data for κ-$(BETS)_2Mn[N(CN)_2]_3$. These data can be obtained free of charge from the Cambridge Crystallographic Data Centre via www.ccdc.cam.ac.uk/data request/cif.

C. Band-structure calculations

The tight-binding band structure was calculated using the extended Hückel method.[19] A modified Wolfsberg-Helmholtz formula was used to calculate the nondiagonal $H_{\mu\nu}$ values.[20] All valence electrons were taken into account in the calculations and the basis set consisted of Slater-type orbitals of double-ζ quality for C 2s and C 2p, S 3s and S 3p, and Se 4s and Se 4p and of single-ζ quality for H. The ionization potentials, contraction coefficients and exponents were taken from previous works.[21]

D. Transport measurements

Sample resistance was measured using a four-probe technique by a lock-in amplifier at 20 Hz alternating current. The samples were thin plates with a characteristic size of $0.5\times0.3\times0.02$ mm^3. The largest surface of the plate was oriented along conducting layers, i.e., parallel to the (bc) plane. Two contacts were attached to each of two opposite sample

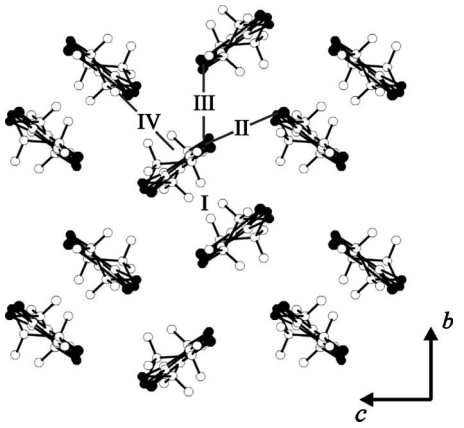

FIG. 1. The radical cation layer of κ-$(BETS)_2Mn[N(CN)_2]_3$ with intermolecular donor···donor interactions inside (i) and between (II, III, and IV) dimers.

surfaces with conducting graphite paste. In the experiment we measured the out-of-plane resistance with the current running mainly perpendicular to conducting layers. Care was taken to eliminate overheating by applied current, which was chosen in the range $(10^{-8}-10^{-5})$ A, depending on the resistive state of the sample. The room-temperature resistivity for all measured samples was about 10^3 Ohm cm in the limits of about 20% and the samples demonstrated the same $R(T)$ dependences. The measurements in the temperature range (1.4–300) K were carried out in a cryostat with a variable temperature insert and under a magnetic field up to 15 T, generated by a superconducting solenoid. The field **B** was directed perpendicular to the sample surface, i.e., along the a^* axis. A ^{4}He gas pressure setup was used for creating homogeneous quasihydrostatic pressure up to 3 kbar and its precise control at low temperatures.

III. RESULTS AND DISCUSSION

A. Temperature-dependent crystal structure

The crystal structure of κ-$(BETS)_2Mn[N(CN)_2]_3$ contains conducting radical-cation layers which alternate along the a direction with polymeric $(Mn[N(CN)_2]_3)^-$ anionic sheets.[16] The structure of the donor layers (Fig. 1) at room temperature is characterized by a disorder in the orientation of terminal ethylene groups in BETS. The relative fractions of BETS molecules in the eclipsed and staggered conformations are 0.20 and 0.80, respectively.[16] When cooling below room temperature the number of staggered conformers gradually increases; at 88 K a completely ordered state with the staggered conformation has been found. No indication of a characteristic temperature of the ordering has been detected.

X-ray diffraction analysis taken at different temperatures around 102 K shows that there is a phase transition associated with an incommensurate superstructure formation: below 102 K x-ray diffraction patterns show weak superstructure reflections which can be described by an incommensurate wave vector $q=0.42\mathbf{b}^*$ (Fig. 2), the superstructure reflections intensities being gradually increased when cooling indicating on the 102 K phase transition temperature. As will be shown below, the transition also clearly affects the transport properties. The superstructure is retained unchanged down to 15 K.

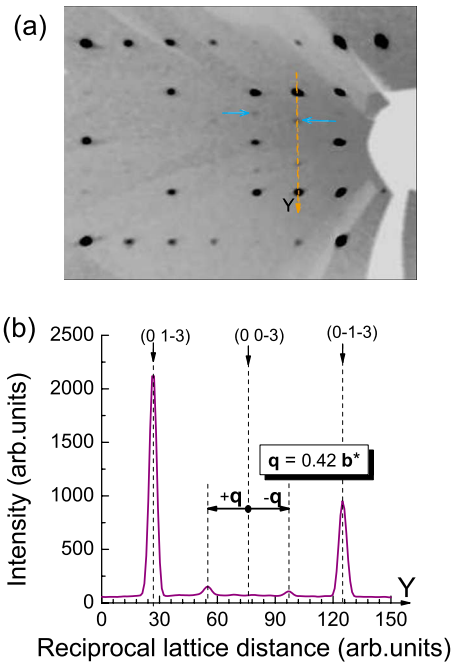

FIG. 2. (Color online) (a) Diffraction pattern in the (a^*,b^*) plane taken at $T=88$ K. The arrows point to satellite reflections; (b) one-dimensional section of the diffraction pattern along the line $Y=k\mathbf{b}^*-3\mathbf{c}^*$.

B. Electronic band structure

The κ-type donor layers in Fig. 1 contain three different types of donor···donor interactions: (i) the intradimer interaction (I), (ii) the interdimer interaction implicating donor molecules which are almost parallel to each other (III), defining chains of dimers along the b direction, and (iii) those associated with donors which are almost orthogonally oriented (II and IV), thus connecting the chains. Table II presents the calculated $|\beta_{HOMO\cdots HOMO}|$ values for every type of HOMO-HOMO interactions along with the density of states at the Fermi level, $n(\epsilon_F)$, for the temperatures 200, 110, 88 and 15 K. One can see that the interactions at different temperatures are remarkably similar despite the progressive

TABLE II. Calculated values of $|\beta_{HOMO\cdots HOMO}|$ [electron volt] for the various nearest-neighbor donor···donor interactions and the density of states at the Fermi level, $n(\epsilon_F)$ [electrons/eV unit cell], for κ-$(BETS)_2Mn[N(CN)_2]_3$.

T (K)	200	110	88	15
I	0.5883	0.6185	0.6196	0.6336
II	0.1293	0.1196	0.1186	0.1153
III	0.3365	0.3407	0.3389	0.3453
IV	0.0373	0.0472	0.0488	0.0532
$n(\epsilon_F)$	8.50	8.41	8.41	8.37

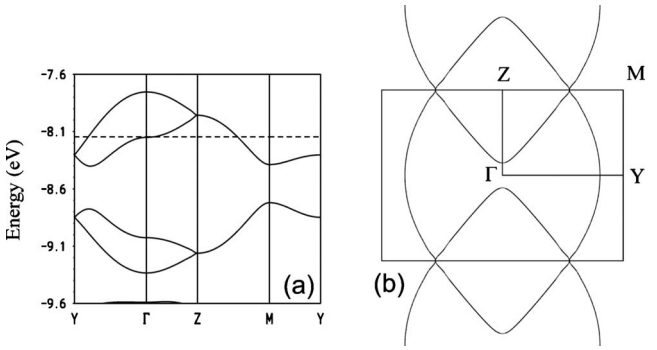

FIG. 3. (a) Calculated band structure for the donor layers of κ-$(BETS)_2Mn[N(CN)_2]_3$ at 110 K. The dashed line refers to the Fermi level and $\Gamma=(0,0)$, $Y=(b^*/2,0)$, $Z=(0,c^*/2)$, and $M=(b^*/2,c^*/2)$; (b) Calculated Fermi surface for the donor layers at 110 K.

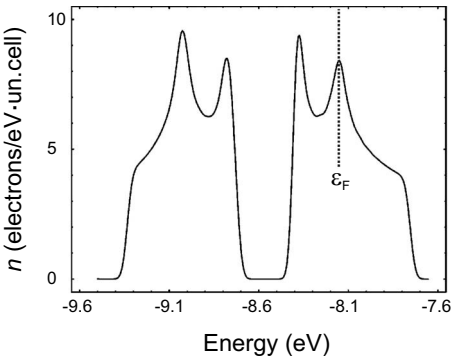

FIG. 4. Calculated density of states for the donor layers at 110 K.

shortening of Se···Se, Se···S, and S···S distances when lowering the temperature. There is only a considerable change between 200 and 110 K (mostly affecting interaction I) although even that is quite small for what is usual in organic conductors. Thus, the electronic structure appears to be quite robust against thermal contraction. The variation in the density of states at the Fermi level is also small. The latter is, however, consistent with a weak thermal compression of the crystal lattice (see Table I).

When these results are compared with those for other κ-type salts,[22] one can notice that the intermolecular interactions along the c axis (i.e., those coupling the chains of dimers) are relatively weak. For example, the $|\beta_{HOMO\cdots HOMO}|$ value for interaction IV at room temperature is only 37 meV, which is three times lower than for another κ salt of BETS with the anion $C(CN)^{3-}$.[23] Therefore, from the point of view of the electronic structure, the present system should better be considered as a series of interacting chains of dimers along the b direction (see Fig. 1). In the usual κ phases the interaction between chains is stronger leading to the typical two-dimensional behavior.

The calculated band structure for the donor lattice at 110 K, i.e., just above the temperature of the transition, is shown in Fig. 3(a). It is the expected band structure for a strongly dimerized κ-type salt. The corresponding Fermi surface is shown in Fig. 3(b). On the whole, its topology is typical of the κ phases: it can be considered as a superposition of large closed pseudoellipses with a cross-section area equal to that of the Brillouin zone. Because of the crystal lattice symmetry, there is no gap at the intersection of the two lines along the $Z\rightarrow M$ line. The area of the closed portion around Z is 27% of the Brillouin zone area. As expected from the very small variation in different interactions for different temperatures, the calculated band structure and Fermi surfaces for the other temperatures are remarkably similar (for instance, the area of the small closed portion of the Fermi surface at 15 K is 26.9%). We note that the crystal structures used for calculating the electronic bands below the transition temperature are, in fact, average structures since the lattice modulation has not been explicitly considered in the refinement. Therefore, the calculations for 88 and 15 K provide only an approximate description of the electronic structure (see below) without taking into account the superstructure potential.

An interesting feature of the Fermi surface shown in Fig. 3(b) is the presence of large flat portions which can be subject to a "hidden nesting."[24] For example, the closed part of the Fermi surface around Z is almost a square. Another feature that distinguishes the present compound from other κ-type salts is that the Fermi level just coincides with a peak in the density of states, as shown in Fig. 4. This does not occur in more isotropic κ-type salts.[25] The reason is that in our compound the flat part of the partially filled band near the Γ point is situated at the Fermi energy [see Fig. 3(a)]. In more isotropic κ salts the band dispersions along the two main directions of the Brillouin zone are more similar and as a result the Γ point is pushed to lower energies; in fact it generally occurs at (or near) the bottom of the band. In the present case, the larger anisotropy of HOMO···HOMO interactions causes (i) a flattening of the partially filled band in a large region around the Γ point and (ii) this variation in band shape relocates the Fermi level almost to the Γ point. These two features lead to the appearance of the peak in the DOS at the Fermi energy. Since in the more isotropic salts the Fermi level lies further away from Γ, small structural changes cannot change the shape of the Fermi surface as it can happen here. Therefore, the present system is expected to be more susceptible to structural changes which may split the peak and thus make the system more stable.

The latter consideration is probably relevant to the transition detected by the x-ray diffraction analysis below 102 K. Indeed, a structural modulation can split the density-of-states peak and lower the system energy even if no full gap is open at the Fermi level. It is important to note that the nesting property of the Fermi surface is not involved in the transition: the experimentally obtained wave vector of the modulation, $\mathbf{q}=0.42\mathbf{b}^*$ is very different from the expected hidden nesting vector $\mathbf{q}_{nesting}\approx 0.48\mathbf{c}^*\pm 0.28\mathbf{b}^*$. While the transition is unlikely to strongly change the total concentration of charge carriers or other electronic properties, it may induce some reconstruction of the Fermi surface. Consequently, the transition does not originate from an electronic instability of the Fermi surface (either charge or spin-density wave). Most likely it is a structural modulation leading to an optimization of the interaction between the donor and anion layers. For instance, even a slight change in the structure may move the

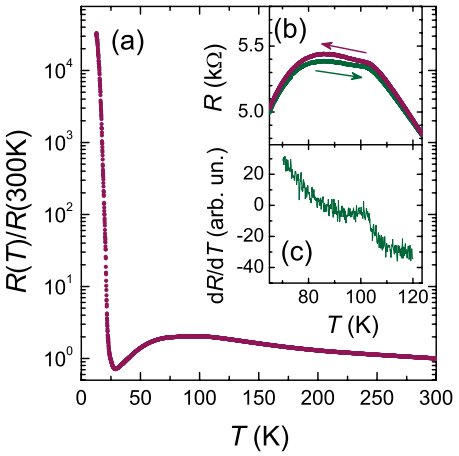

FIG. 5. (Color online) (a) Normalized interlayer resistance of κ-$(BETS)_2Mn[N(CN)_2]_3$ as a function of temperature; (b) Down- and upward temperature sweeps of the resistance around the structural transition. One can see a hysteresis below the resistance anomaly at $T=102$ K; (c) Temperature derivative of R_c showing a discontinuous change at 102 K.

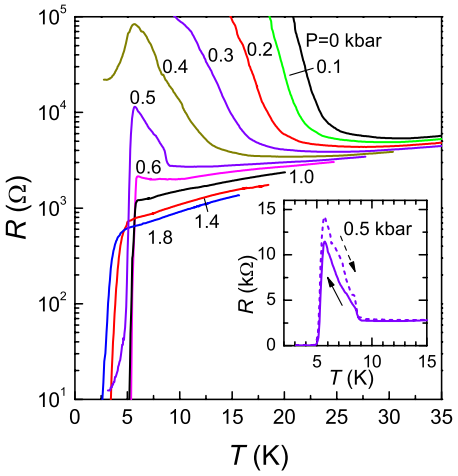

FIG. 6. (Color online) Temperature-dependent interlayer resistance at pressures between 0 and 1.8 kbar. The metal-insulator transition is gradually suppressed with increasing pressure and is ultimately replaced by the superconducting transition. The inset illustrates a hysteresis between up- and downward temperature sweeps in the region of coexistence of the insulating and metallic states.

flat part of the electronic dispersion near Γ away from the Fermi level, thus transforming the closed part of the Fermi surface centered at Z into a pair of corrugated open sheets extended along $\Gamma \rightarrow Z$ line. Further, the modulation may disturb the original crystal symmetry, removing the degeneracy at the Fermi level along the $Z \rightarrow M$ line. In addition, the incommensurate superstructure leads to folding of the Fermi surface and thus creation of weak gaps at the Fermi surface crossings. That the Fermi surface is, indeed, reconstructed at low temperatures will be seen from the Shubnikov-de Haas (SdH) data presented below.

C. *T-P* phase diagram

The temperature-dependent out-of-plane resistance of a single crystal of κ-$(BETS)_2Mn[N(CN)_2]_3$ at ambient pressure is shown in Fig. 5. The figure displays several interesting features. First, the $R(T)$ dependence shows a wide hump at around $T_h \sim 85$ K, which has been associated with a breakdown of the interlayer transport coherence at $T > T_h$ and strong electron-phonon interactions[16]. Another feature in the temperature dependence of interlayer resistance is a sharp bending at $T \approx 102$ K accompanied by a hysteresis in the temperature range of 80–100 K (see insets in Fig. 5). This anomaly is obviously a manifestation of the structural transition detected by the x-ray analysis. Finally, in the low-temperature region, the resistance reaches a minimum at $T_M \cong 27$ K followed by a dramatic increase, indicating a metal-insulator transition.[16]

The latter transition cannot be attributed to a structural transformation, as the crystal structure at $T=15$ K, i.e., well below T_M, is the same as at higher temperatures (see Sec. III A). Therefore, its explanation should be based on intrinsic properties of the electronic system. A possible mechanism is associated with strong electron correlations driving the system into the Mott insulating state.[26,27] Indeed, like the known BEDT-TTF-based Mott-insulating κ-type salts, the present compound is characterized by a rather weak band dispersion and a strong dimerization of the organic donor molecules (see Sec. III B), which leads to an effectively half-filled conducting band. Alternatively, one could consider a charge- or spin-density wave formation, taking into account the above mentioned hidden nesting property of the Fermi surface. However, the nesting can close only a fraction of the Fermi surface, the pseudosquare centered at point Z [see Fig. 3(b)], leaving a large part of charge carriers metallic. This is obviously inconsistent with the insulating character of the low-temperature state: the resistance grows by five orders of magnitude upon cooling from T_M to 15 K. A further possibility would be to relate the metal-insulator transition to an influence of the magnetically ordered anion sublattice on the conducting system, as it was suggested for λ-$(BETS)_2FeCl_4$.[28] However, no clear evidence of magnetic ordering of Mn^{2+} spins in the anion sublattice have been found near the transition temperature.[16] Thus, the Mott instability driven by electron correlations in the conducting system seems to be the most likely mechanism of the observed metal-insulator transition in κ-$(BETS)_2Mn[N(CN)_2]_3$. Of course, further work needs to be done to verify this scenario.

As reported earlier,[16] the metal-insulator transition is suppressed if the sample is cooled in a drop of silicone oil. This suggests high sensitivity of the electronic ground state to pressure. To obtain more quantitative information, we have carried out a systematic study of magnetotransport properties of our samples under pressure. The influence of pressure on $R(T)$ curves is shown in Fig. 6. One can see that the temperature of the metal-insulator transition rapidly decreases with increasing pressure. At pressure $P=0.4$ kbar, a resistive drop associated with a partial superconducting transition is observed starting from 5.7 K. The drop becomes more pronounced as the pressure increases. At $P=0.6$ kbar, resistance exhibits a rather sharp transition to zero with the midpoint at $T_c=5.75$ K and a width (defined as the difference between

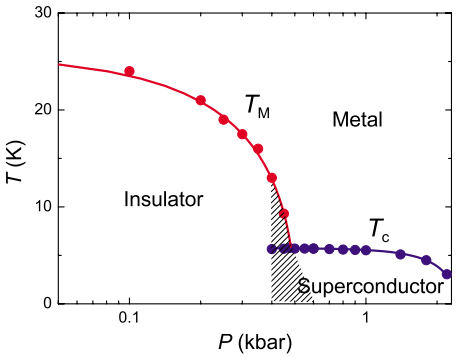

FIG. 7. (Color online) The T-P phase diagram. The hatched area shows the region where the metallic/superconducting and insulating phases coexist.

the temperatures corresponding to 0.95 and 0.05 of the resistance value at the transition onset) of 0.4 K. The transition is, however, preceded by a slight upturn of the resistance, indicating the presence of the insulating phase. The coexistence of the insulating and metallic/superconducting phases at $P=(0.4-0.6)$ kbar implies that the transition between the two states is of the first order in this pressure range. This is corroborated by a notable hysteresis in the $R(T)$ dependence in the transition region, as shown in the inset in Fig. 6. We note that the first order phase transition from metallic and Mott-insulating states has also been found on another organic conductor κ-(BEDT-TTF)$_2$Cu[N(CN)$_2$]Cl.[6]

The low-temperature phase diagram of κ-(BETS)$_2$Mn[N(CN)$_2$]$_3$ is summarized in Fig. 7, demonstrating the regions of the insulating, metallic, and superconducting states. The temperature of the metal-insulator transition steadily goes down with increasing pressure. This behavior can qualitatively be explained by a pressure-induced broadening of the conducting band, which results in weakening the electron correlations and thereby suppresses the Mott instability.

By contrast to $T_M(P)$, the superconducting transition temperature stays nearly constant between 0.4 and 1.0 kbar. This apparent insensitivity of the superconducting transition looks very atypical for an organic superconductor.[29] For example, the suppression rate $dln(T_c)/dP \approx 0.3$ kbar^{-1} is observed on κ-(BEDT-TTF)$_2$Cu(NCS)$_2$. Note, however, that at pressures above 1 kbar T_c begins to decrease rapidly. One can suggest that flattening of $T_c(P)$ at $P<1$ kbar is due to proximity of the insulating transition. Without the insulating instability T_c would increase when lowering the pressure; however, coming closer to the metal-insulator phase boundary, the superconducting state becomes less stable and T_c does not show the expected increase.

D. Magnetoresistance and Shubnikov-de Haas oscillations under pressure

Figure 8 shows the magnetic field dependence of the low-temperature interlayer resistance of a κ-(BETS)$_2$Mn[N(CN)$_2$]$_3$ sample at different pressures. The field is applied perpendicular to the conducting layers. One can see that the superconducting state is rapidly suppressed

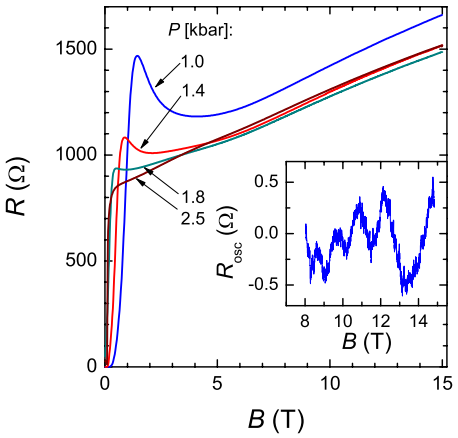

FIG. 8. (Color online) Magnetic field dependence of the interlayer resistance at pressures 1.0 to 2.5 kbar. The field is applied perpendicular to conducting layers; $T=1.4$ K. The inset shows the oscillating magnetoresistance component for $P=1.0$ kbar, obtained by subtracting the monotonic background from the raw data.

by the field. At pressures $P<2$ kbar, the magnetoresistance exhibits a maximum followed by a negative slope in the intermediate field range. The reason for this negative slope is still to be clarified. On the one hand, it resembles the behavior observed on other layered superconductors and attributed to fluctuation effects in the interlayer transport in a system of weakly coupled superconducting layers.[30–33] The fact that the negative slope weakens at increasing pressure and eventually disappears above 2 kbar could be explained by a pressure induced enhancement of the interlayer coupling. On the other hand, at this stage we cannot rule out the possibility that some remnants of the insulating phase are still present at pressures up to 2 kbar and the effect of magnetic field is to suppress the strongly weakened insulating state in this minor volume fraction. Further experiments are planned to address this issue.

At further increasing field, the negative contribution to magnetoresistance saturates, leading to a conventional positive slope. At $B>(8-9)$ T weak ($R_{osc}/R \leq 5\times10^{-4}$) oscillations, were detected. As an example, the oscillatory magnetoresistance component obtained after subtracting a low-order polynomial fit from the raw experimental curve for $P=1$ kbar is plotted in the inset in Fig. 8. The oscillations are periodic in the inverse magnetic field scale, as illustrated by Fig. 9. This behavior is characteristic of the SdH oscillations:[34] in effect, the number N on the right-hand side of Fig. 9 represents the sequence number of a Landau tube crossing the Fermi surface of this quasi-two-dimensional metal at a given field.[35]

The frequency of the SdH oscillations provides a direct measure of the area of the relevant closed Fermi surface in the plane of conducting layers.[34,35] We determined the frequency both from the slope of the linear $N(1/B)$ dependence and from the Fourier analysis. The difference between the values determined by these two methods did not exceed (2–3)%. For the oscillations presented in Fig. 9, obtained at a pressure $P=1.0$ kbar, the frequency $F=(88\pm1)$ T corresponds to a very small area, $(8.4\pm0.1)\times10^{17}$ m^{-2}, or just about 2.2% of the first Brillouin-zone area. The Fermi sur-

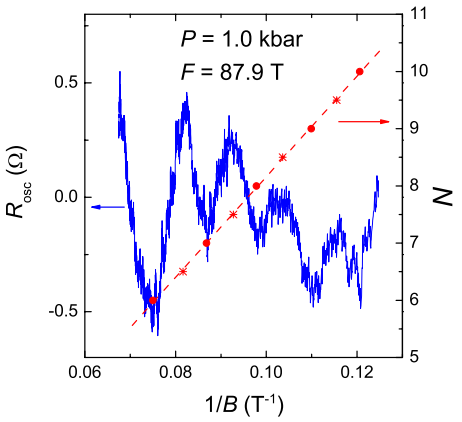

FIG. 9. (Color online) The same data as in the inset in Fig. 8 replotted in the inverse field scale (solid line). The oscillations are periodic, as illustrated by the linear dependence of the oscillation index N, integer for dips in R_{osc} and odd half integer for peaks (circles and stars, respectively) on $1/B$.

face shown in Fig. 3(b) does not possess small pockets which could be attributed to the present oscillations. However, as noted above, this Fermi surface was obtained from the calculations which did not take into account the incommensurate lattice modulation arising at 102 K. The modulation potential imposed on the electronic system should fold the original Fermi surface and open new gaps, producing new small closed pockets. A similar transformation was invoked to explain slow SdH oscillations in κ-(BEDT-TTF)$_2$Cu[N(CN)$_2$]Br,[36] which also undergoes a transition at about 200 K involving the appearance of a superstructure. We, thus, consider the slow SdH oscillations in the present salt as an evidence for a reconstruction of the Fermi surface due to the incommensurate structural modulation.

Using the standard Lifshitz-Kosevich analysis,[34] we have estimated the effective cyclotron mass of the charge carriers responsible for the oscillations from the temperature dependence of the oscillation amplitude. The experimental data and mass plot for pressure $P=1.8$ kbar are shown in Fig. 10. The oscillation amplitudes used in Fig. 10(b) were determined from fast Fourier spectra of the $R_{osc}(1/B)$ patterns shown in Fig. 10(a) for different temperatures. The value obtained, $m_c \approx 0.9m_0$ (where m_0 is the free-electron mass), is quite high, taking into account the very small size of the relevant Fermi surface. It can, at least partly, be explained by the rather flat band dispersion and, hence, large density of states at the Fermi level as predicted by the band-structure calculations (see Fig. 4). At present we cannot unambiguously assign the observed SdH oscillations to a specific cross section of the reconstructed Fermi surface and evaluate the relevant cyclotron mass from the band-structure calculations. However, we can compare the experimentally obtained value m_c with the mass $m_b=1.3m_0$ estimated for the much larger closed portion of the unreconstructed Fermi surface, centered at point Z on the Brillouin zone boundary [Fig. 3(b)]. The fact that the two values are comparable with each other, despite the large, a factor of 10, difference in the size of the corresponding Fermi surfaces, implies a significant role of

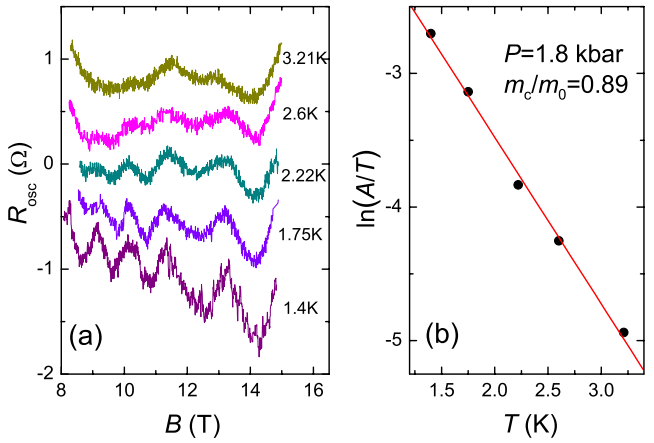

FIG. 10. (Color online) (a) SdH oscillations for different temperatures, at $P=1.8$ kbar; (b) Temperature dependence of the logarithm of the oscillation amplitude A divided by T. The solid line is a fit to the Lifshitz-Kosevich theory (Ref. 34), yielding the effective cyclotron mass $m_c=0.89m_0$.

many-body interactions in renormalizing the effective cyclotron mass.[35] In our case this renormalization is most likely associated with strongly enhanced electron correlations in the vicinity of the metal-insulator transition.

The pressure dependences of the oscillation frequency and the cyclotron mass are presented in Fig. 11. The frequency grows by about 10% when increasing pressure from 1.0 to 2.5 kbar. This is a relatively large change but it is not unprecedented for the organic κ-type salts[36–38] and likely originates from an anisotropic compression of the crystal lattice. The cyclotron mass is also found to increase in a similar manner in the interval between 1.0 and 2.5 kbar. This is, however, an unexpected result. Usually a pressure applied to an organic conductor increases the conduction bandwidth, thereby weakening many-body interactions and reducing the renormalized cyclotron mass.[37] As seen from Fig. 7, at increasing pressure we, indeed, move away from the metal-insulator transition, which should lead to a decrease in electronic correlations. Therefore, the positive slope of the $m_c(P)$

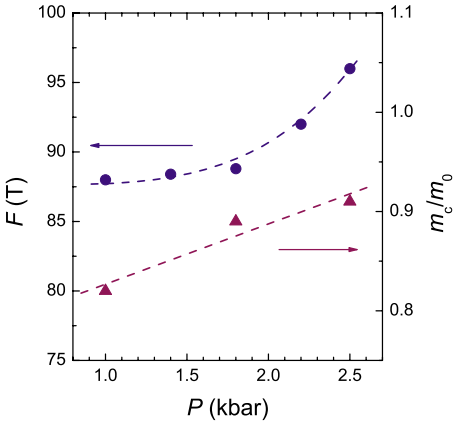

FIG. 11. (Color online) Pressure dependence of the oscillation frequency (circles; scale on the left-hand side) and cyclotron mass (triangles; scale on the right-hand side). Dashed lines are guide for the eyes.

dependence looks surprising and needs to be clarified in future studies.

IV. CONCLUSION

We have performed studies of the temperature-dependent crystal and electronic band structures as well as transport properties of the new layered molecular conductor κ-$(BETS)_2Mn[N(CN)_2]_3$ possessing localized spins in the insulating anion layers. We have found a phase transition near 102 K resulting in the formation of incommensurate superstructure below 102 K. The transition is reflected in a weak anomaly in the electrical resistivity and leads to a topological reconstruction of the Fermi surface revealed by slow SdH oscillations. However, the origin of the transition lies most likely in optimization of the interactions between the donor and acceptor layers rather than in the electronic structure of the donor layers. The low-temperature metal-insulator transition is found to be unrelated to structural changes and, thus, associated with the properties of the conducting system. The weak dispersion of charge carriers, corroborated by heavy effective cyclotron mass found in the SdH measurements, implies that electronic correlations play an important role in the system. This, along with the strong dimerization of the donor molecules suggests the electronic ground state to be a Mott insulator. Based on resistive measurements under pressure, we have built a *T*-*P* phase diagram of the compound, incorporating insulating, metallic, and superconducting states. At pressures around the critical value at which the insulating state is suppressed, the metal-insulator transition is found to be of the first order. Finally, no direct signatures of interaction between localized spins of Mn^{2+} in the insulating layers and itinerant spins in the donor layers have been found in this work. Keeping in mind distinct anomalies in magnetic susceptibility near the metal-insulator transition and at lower temperatures reported earlier,[16] further magnetic studies, including those under pressure, are highly desirable to clarify this issue.

ACKNOWLEDGMENTS

We are grateful to A. Kobayashi and H. Kobayashi for providing us with the BETS donor. This work was partially supported by the RFBR under Grants No. 09-02-00852, No. 09-02-00241, No. 07-02-91562, DFG under Grant No. RUS 113/926/0-1, and the Program of Russian Academy of Sciences. Work at Bellaterra was supported by DGES-Spain (under Projects No. FIS2009-12721-C04-03 and No. CSD2007-00041).

[1] *Handbook on High-Temperature Superconductivity: Theory and Experiment*, edited by J. R. Schriefer and J. S. Brooks (Springer, New York, 2007).
[2] D. C. Johnston, Adv. Phys. **59**, 803 (2010).
[3] *The Physics of Organic Superconductors and Conductors*, Springer Series in Materials Science Vol. 110, edited by A. G. Lebed (Springer-Verlag, Berlin, 2008).
[4] *Heavy Fermion Systems*, Handbook of Metal Physics, edited by P. Misra (Elsevier, Amsterdam, 2002).
[5] K. Kanoda, J. Phys. Soc. Jpn. **75**, 051007 (2006).
[6] P. Limelette, P. Wzietek, S. Florens, A. Georges, T. A. Costi, C. Pasquier, D. Jérome, C. Mézière, and P. Batail, Phys. Rev. Lett. **91**, 016401 (2003).
[7] F. Kagawa, K. Miyagawa, and K. Kanoda, Nature (London) **436**, 534 (2005).
[8] Y. Shimizu, K. Miyagawa, K. Kanoda, M. Maesato, and G. Saito, Phys. Rev. Lett. **91**, 107001 (2003).
[9] M. Yamashita, N. Nakata, Y. Kasahara, T. Sasaki, N. Yoneyama, N. Kobayashi, S. Fujimoto, T. Shibauchi, and Y. Matsuda, Nat. Phys. **5**, 44 (2009).
[10] T. Ishiguro, R. Yamaji, and G. Saito, *Organic Superconductors* (Springer-Verlag, Berlin, 1988); E. Coronado and P. Day, Chem. Rev. **104**, 5419 (2004); T. Enoki and A. Miyazaki, *ibid.* **104**, 5449 (2004); H. Kobayashi, H. Cui, and A. Kobayashi, *ibid.* **104**, 5265 (2004); L. Ouahab, *Organic Conductors, Superconductors and Magnets: From Synthesis to Molecular Electronics*, edited by L. Ouahab and E. Yagubskii (Kluwer Academic, Dordrecht/Boston/London, 2003), p. 99; G. Saito and Y. Yoshida, Bull. Chem. Soc. Jpn. **80**, 1 (2007); E. Coronado and K. R. Dunbar, Inorg. Chem. **48**, 3293 (2009); L. Ouahab and T. Enoki, Eur. J. Inorg. Chem. **2004**, 933 (2004).
[11] M. Kurmoo, A. W. Graham, P. Day, S. J. Coles, M. B. Hursthouse, J. L. Caulfield, J. Singleton, F. L. Pratt, W. Hayes, L. Ducasse, and P. Guionneau, J. Am. Chem. Soc. **117**, 12209 (1995); S. Rashid, S. S. Turner, P. Day, J. A. K. Howard, P. Guionneau, E. J. L. McInnes, F. E. Mabbs, R. J. H. Clark, S. Firth, and T. J. Biggs, J. Mater. Chem. **11**, 2095 (2001); A. Audouard, V. N. Laukhin, L. Brossard, T. G. Prokhorova, E. B. Yagubskii, and E. Canadell, Phys. Rev. B **69**, 144523 (2004).
[12] T. Otsuka, A. Kobayashi, Y. Miyamoto, J. Kiuchi, S. Nakamura, N. Wada, E. Fujiwara, H. Fujiwara, and H. Kobayashi, J. Solid State Chem. **159**, 407 (2001).
[13] E. Ojima, H. Fujiwara, K. Kato, H. Kobayashi, H. Tanaka, A. Kobayashi, M. Tokumoto, and P. Cassoux, J. Am. Chem. Soc. **121**, 5581 (1999).
[14] S. Uji, H. Shinagawa, T. Terashima, T. Yakabe, Y. Terai, M. Tokumoto, A. Kobayashi, H. Tanaka, and H. Kobayashi, Nature (London) **410**, 908 (2001).
[15] H. Fujiwara, H. Kobayashi, E. Fujiwara, and A. Kobayashi, J. Am. Chem. Soc. **124**, 6816 (2002).
[16] N. D. Kushch, E. B. Yagubskii, M. V. Kartsovnik, L. I. Buravov, A. D. Dubrovskii, A. N. Chekhlov, and W. Biberacher, J. Am. Chem. Soc. **130**, 7238 (2008).
[17] Oxford Diffraction, 2007. Oxford Diffraction Ltd., Xcalibur CCD system, CRYSALISPRO software system, version 1.171.32.
[18] G. M. Sheldrick, Acta Crystallogr., Sect. A: Found. Crystallogr. **64**, 112 (2008).
[19] M.-H. Whangbo and R. Hoffmann, J. Am. Chem. Soc. **100**, 6093 (1978).
[20] J. Ammeter, H.-B. Bürgi, J. Thibeault, and R. Hoffmann, J. Am.

Chem. Soc. **100**, 3686 (1978).
[21] A. Pénicaud, K. Boubekeur, P. Batail, E. Canadell, P. Auban-Senzier, and D. Jérome, J. Am. Chem. Soc. **115**, 4101 (1993); A. Pénicaud, P. Batail, C. Coulon, E. Canadell, and C. Perrin, Chem. Mater. **2**, 123 (1990).
[22] A. M. Kini, U. Geiser, H. H. Wang, K. D. Carlson, J. M. Williams, W. K. Kwok, K. G. Vandervoort, J. E. Thompson, D. L. Stupka, D. Jung, and M.-H. Whangbo, Inorg. Chem. **29**, 2555 (1990).
[23] B. Z. Narymbetov, N. D. Kushch, L. V. Zorina, S. S. Khasanov, R. P. Shibaeva, T. G. Togonidze, A. E. Kovalev, M. V. Kartsovnik, L. I. Buravov, E. B. Yagubskii, E. Canadell, A. Kobayashi, and H. Kobayashi, Eur. Phys. J. B **5**, 179 (1998).
[24] M.-H. Whangbo, J. Ren, W. Liang, E. Canadell, J. P. Pouget, S. Ravy, J. M. Williams, and M. A. Beno, Inorg. Chem. **31**, 4169 (1992).
[25] A. J. Schultz, H. H. Wang, J. M. Williams, L. W. Finger, R. M. Hazen, C. Rovira, and M.-H. Whangbo, Physica C **234**, 300 (1994).
[26] H. Kino and H. Fukuyama, J. Phys. Soc. Jpn. **64**, 2726 (1995).
[27] R. H. McKenzie, Comments Condens. Matter Phys. **18**, 309 (1998).
[28] L. Brossard, R. Clérac, C. Coulon, M. Tokumoto, T. Ziman, D. K. Petrov, V. N. Laukhin, M. J. Naughton, A. Audouard, F. Goze, A. Kobayashi, H. Kobayashi, and P. Cassoux, Eur. Phys. J. B **1**, 439 (1998).
[29] N. Toyota, M. Lang, and J. Müller, *Low-Dimensional Molecular Metals* (Springer, Berlin, Heidelberg, 2007).
[30] F. Zuo, J. A. Schlueter, M. E. Kelly, and J. M. Williams, Phys. Rev. B **54**, 11973 (1996).
[31] S. Friemel, C. Pasquier, and D. Jérome, Physica C **292**, 273 (1997).
[32] M. V. Kartsovnik, G. Yu. Logvenov, K. Maki, and N. D. Kushch, Synth. Met. **103**, 1827 (1999).
[33] X. Su, F. Zuo, J. A. Schlueter, J. M. Williams, P. G. Nixon, R. W. Winter, and G. L. Gard, Phys. Rev. B **59**, 4376 (1999).
[34] D. Shoenberg, *Magnetic Oscillations in Metals* (Cambridge University Press, Cambridge, 1984).
[35] M. Kartsovnik, Chem. Rev. **104**, 5737 (2004).
[36] H. Weiss, M. V. Kartsovnik, W. Biberacher, E. Steep, E. Balthes, A. G. M. Jansen, K. Andres, and N. D. Kushch, Phys. Rev. B **59**, 12370 (1999).
[37] J. Caulfield, W. Lubczynski, F. L. Pratt, J. Singleton, D. Y. K. Ko, W. Hayes, M. Kurmoo, and P. Day, J. Phys.: Condens. Matter **6**, 2911 (1994).
[38] M. V. Kartsovnik, W. Biberacher, K. Andres, and N. D. Kushch, Pis'ma Zh. Eksp. Teor. Fiz. **62**, 890 (1995) [JETP Lett. **62**, 905 (1995)].